Localized interface states in coherent isovalent semiconductor heterojunctions

Voicu Popescu[1,2,*] and Alex Zunger[3,†]

[1]*Physics Department and REMRSEC, Colorado School of Mines, Golden, Colorado 80401, USA*
[2]*National Renewable Energy Laboratory, Golden, Colorado 80401, USA*
[3]*University of Colorado, Boulder, Colorado 80302, USA*

(Received 13 April 2011; published 16 September 2011; publisher error corrected 22 September 2011)

Interface states can occur in semiconductor heterojunctions whenever a significant perturbation is present across the interface, for example, interface defects, lattice mismatch, change of sign in the effective mass, or sharp variations in the potential. We discuss here a different type of natural interface states appearing in perfectly coherent and isovalent III–V heterojunctions even in the absence of such extreme perturbations. Using atomistic empirical pseudopotential calculations we find that this is a general phenomenon occurring whenever the junction is formed by two semiconductors having their respective conduction band minima in two different valleys which: (i) fold into the same $\vec{q}$ point of the two-dimensional Brillouin zone and (ii) are allowed by symmetry to couple at this point $\vec{q}$. In this case, the system manifests two potential wells of opposite attractiveness, such as a well for Γ states and a barrier for X states. For InP/GaP this leads to the formation of an interface-localized state already in a single heterojunction, lying energetically between the Γ edge of InP and the X edge of GaP. When the InP/GaP quantum well is formed, this single state evolves into a pair of interface-localized states, located deep in the band gap. Because of their mixed Γ-X character, these interface-localized states possess a strong optical signature. This new understanding allows us to provide a different interpretation to the previously observed photoemission data for InP/GaP quantum wells and dots. We find analogous states in GaAs/AlAs and GaAs/GaP but now these levels are resonant within the continuum of states of the matrix conduction band and are therefore less pronounced.

DOI: 10.1103/PhysRevB.84.125315 PACS number(s): 73.20.−r, 73.22.−f, 71.55.Eq

I. INTRODUCTION: INTRINSIC VERSUS EXTRINSIC INTERFACE STATES

Whereas the interface between a semiconductor and vacuum represents a significant perturbation on the crystalline potential, often leading to the formation of localized surface states,[1] the interface between two semiconductors corresponds to a weaker perturbation and, in general, does not lead to such a manifestation. Exceptions include interfaces between electronically nonisovalent IV/III–V or III–V/II–VI components, for example, Ge/GaAs (Ref. 2) and GaAs/ZnSe (Ref. 3), or isovalent but structurally highly mismatched systems, such as Si/Sn (Ref. 4) or CdTe/ZnTe (Ref. 5).

Precisely because of this reason—lack of localized interface states in the energy range of interest—heterojunctions between electronically and structurally closely matched semiconductors (isovalent and coherently strained) have long formed the basis for successful heterostructure and superlattice devices.[6] Exceptions involve unusual cases such as an interface between two (isovalent and coherent) semiconductors having opposite effective masses like HgTe/CdTe.[7,8] Here we discuss an important exception to this tradition: the predicted existence of natural, localized interface states for isovalent and isostructural components even in the absence of opposite effective masses (inversed band systems) or any interface defects or lattice incoherence.

An example is shown in Fig. 1 for an $(\mathrm{InP})_n/\mathrm{GaP}(001)$ quantum well (QW), where calculated atomistic pseudopotential conduction band (electron) wave functions are plotted along the (001) directions for several thickness values n. For $n \leqslant 10$ the two lowest electron states of the QW are IF_1 and IF_2 that are strongly localized at the interface. As it turns, these states have a nonzero *bulk* Γ character (denoted as $\%\Gamma$ in the top right corner of each panel in Fig. 1). Concomitantly, the optical transitions from the QW valence band (VB) states (localized naturally inside the InP well) to these interface-localized states (a spatially indirect transition) are rather strong, as seen in the calculated interband absorption spectra shown in Fig. 2. Thus, we encounter here interface localization at structurally perfect interfaces between isovalent semiconductor components, optically allowed from the VB, despite spatial indirectness.

We find that such "natural interface states" in the conduction band (CB) are a general phenomenon occurring whenever the junction is formed by two semiconductors having their respective conduction band minima (CBM) in two different valleys which fold into the same $\vec{q}$ point of the two-dimensional Brillouin zone where, in addition, they are symmetry-allowed to couple. In this case, the system manifests two potential wells of opposite attractiveness, such as a well for Γ states and a barrier ("anti-well") for X states which leads to the formation of an interface-localized state (IFLS) already in a *single* heterojunction, as shown in Fig. 3. This type of localization is different from other mechanisms, which underlie symmetry-governed coupling and/or segregation, which occur in thin superlattices.[9]

We show that the IFLSs appearing in $(\mathrm{InP})_n/\mathrm{GaP}$ QWs are consistent with the observed photoluminescence (PL) measurements on ultrathin $(\mathrm{InP})_n/\mathrm{GaP}$ QWs ($n \simeq 0.8-1.5$ monolayers) of Hatami *et al.*[10] Time-resolved PL on these samples showed a peculiar long decay time, characteristic to type II transitions. Furthermore, effective mass modeling showed that no confined Γ state can exist for such thin QWs, leading the authors to conclude that the PL is the result of some indirect transitions in both real and reciprocal space. Our

 ©2011 American Physical Society

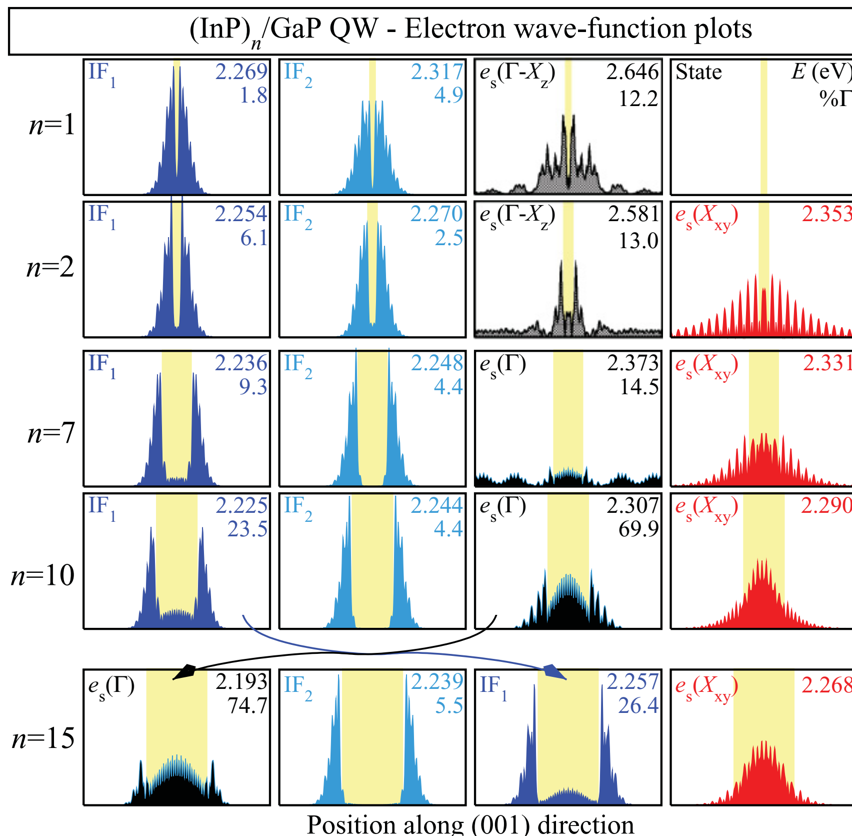

FIG. 1. (Color online) In-plane average density of selected electron wave functions along the (001) growth direction in $(\mathrm{InP})_n/\mathrm{GaP}$ quantum well (QW), calculated for different numbers of monolayers (MLs) n. From top to the bottom, $n = 1$, 2, 7, 10, and 15 MLs. The yellow (light gray) shaded area marks the position of the InP QW. We indicate in the figure the designation of each state [IF_1, IF_2, $e_s(\Gamma - X_z)$, $e_s(\Gamma)$, and $e_s(X_{xy})$] and its energy relative to the unstrained GaP valence band maximum (VBM, -6.099 eV). For QW states resulting from the folding of bulk states along the $\Gamma - X_z$ direction we also give the amount of their Γ character. The GaP conduction band minimum (CBM) edge is at 2.363 eV. Note the change in energetic position of IF_1 and $e_s(\Gamma)$ occurring between $n = 10$ MLs and $n = 15$ MLs.

results suggest instead that the transitions involve IFLSs with a nonzero, relatively large Γ character (which gives them a strong oscillator strength), yet manifesting spatial indirectness (which prolongs the decay time). We find that under the general circumstances described in this paper such coherent interfaces produce localized interface states with strong transitions that are spatially indirect but quasidirect in momentum space. Indeed, this new type of "natural" interface state due to the existence of a Γ well and an X_z antiwell is predicted to exist also in other isovalent interfaces, except that often, for example $(\mathrm{GaAs})_n/\mathrm{AlAs}$ and $(\mathrm{GaAs})_n/\mathrm{GaP}$, these states are resonant within the continuum (above the barrier CBM) and thus, unlike the case of $(\mathrm{InP})_n/\mathrm{GaP}$, their manifestation is less dramatic.

II. FOLDING AND COUPLING OF BULK STATES IN SUPERLATTICES

Folding and coupling of folded states in a superlattice are sequential steps that need to be understood separately. While folding is the result of a geometric construction and depends just on the general symmetry of the wave vectors described by the Brillouin zone (BZ), the coupling of folded states reflects the individual symmetries of the eigenstates. This section describes these two steps separately; going from the case of a general superlattice (SL) to the particular case of an (001)-oriented one and then treating two cases of coupling manifesting in the latter.

The alternating layers of two materials AB and CD forming a SL or a QW modify the symmetry of the parent lattice along the growth direction $\vec{n}$. It is the reason why theoretical descriptions of such systems use large supercells which are made of several bulk unit cells stacked along $\vec{n}$, leading to the sequence $(\mathrm{AB})_n/(\mathrm{CD})_m$, with (n,m) finite for SLs and $m \to \infty$ for QWs. A direct consequence of such a construction—supercell commensurate with the bulk unit cell—is that any SL/QW state $|\vec{K}\nu\rangle$ of band index ν and wave vector $\vec{K}$ in the supercell BZ can be written as a linear combination of $(n+m)$ *bulk* states $|\vec{k}_i\mu\rangle$ of band index μ and wave vector $\vec{k}_i$ $(i = 1,\ldots,n+m)$ of the parent bulk BZ.[9,11] Commonly termed as *folding* of the bulk BZ into the supercell BZ, this is formally expressed by

$$|\vec{K}\nu\rangle = \sum_{i}^{n+m}\sum_{\mu} A(\vec{k}_i\mu;\vec{K}\nu)\,|\vec{k}_i\mu\rangle. \quad (1)$$

The folding bulk vectors $\vec{k}_i$ are determined by the supercell size used to describe the SL or QW system and by its growth direction $\vec{n}$. Denoting by $\vec{G}$ the shortest bulk reciprocal lattice vector parallel to $\vec{n}$, the bulk vectors $\vec{k}_i$ folding into a supercell wave vector $\vec{q}$ are[11]

$$\vec{k}_i = \vec{q} + \frac{i}{(n+m)}\vec{G}, \quad \text{with} \quad i = -\frac{n+m}{2}+1,\ldots,\frac{n+m}{2}. \quad (2)$$

The linear combination given by Eq. (1) is generally valid and can be used to analyze any supercell state $|\vec{K}\nu\rangle$ in terms of its bulk components.[12]

Folded bulk states may also couple one to another if they have the same symmetry in the supercell BZ. This coupling of the folded states reflects the change in the individual symmetries of the bulk eigenstates in the larger system. States

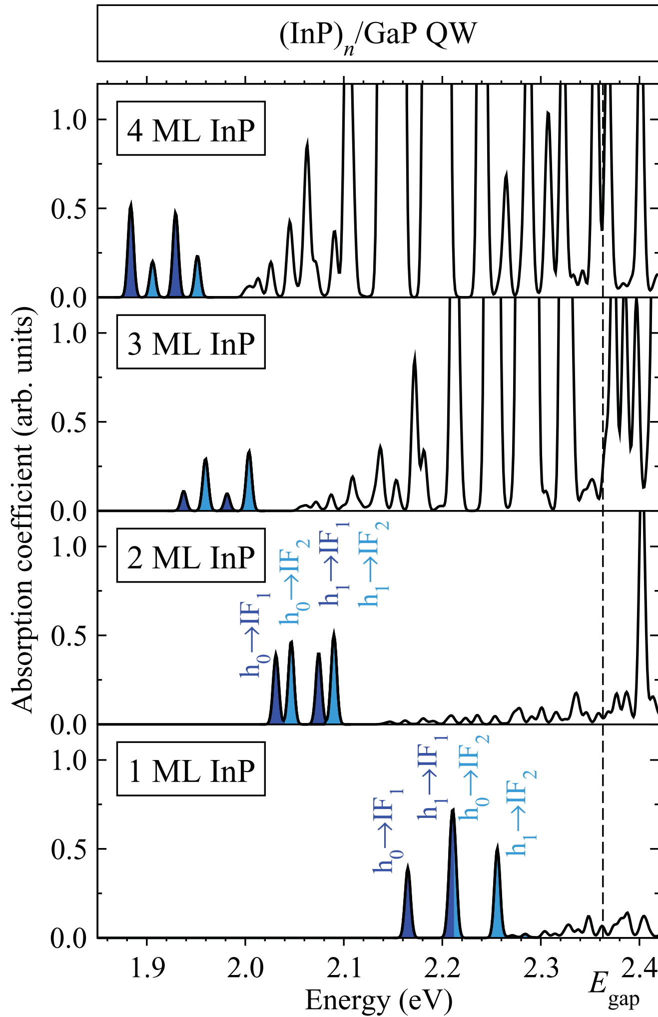

FIG. 2. (Color online) Single-particle interband absorption spectra for thin $(\mathrm{InP})_n$/GaP QW, $n = 1, \ldots, 4$ MLs. The lowest allowed transitions are from the highest QW-confined hole levels (h_0 and h_1) to the interface-localized states IF_1 and IF_2, and are highlighted by shaded peaks. Note the close coincidence of the $h_0 \mapsto \mathrm{IF}_2$ and $h_1 \mapsto \mathrm{IF}_1$ transitions for $n = 1$ ML. For thicker QWs, all peaks separate, maintaining the order $h_0 \mapsto \mathrm{IF}_1$, $h_0 \mapsto \mathrm{IF}_2$, $h_1 \mapsto \mathrm{IF}_1$, $h_1 \mapsto \mathrm{IF}_2$. Energies are given relative to the unstrained GaP VBM (−6.099 eV).

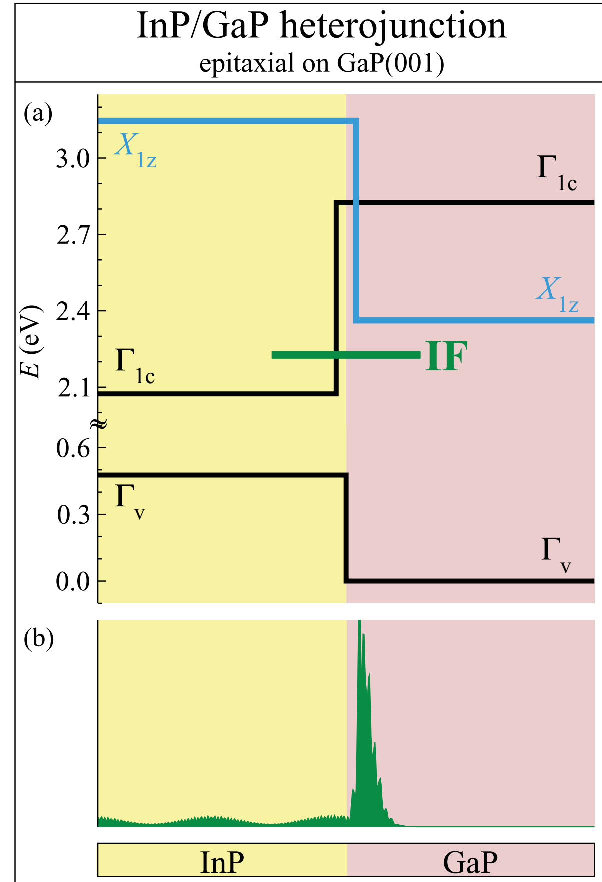

FIG. 3. (Color online) Results of atomisitic empirical pseudopotential calculations for the InP/GaP single heterojunction epitaxially strained to GaP(001). (a) Valence Γ_v and conduction band (CB) Γ_c and X_z offsets between the strained InP and the unstrained GaP. The offset of the Γ_c and X_z CB valleys leads to the appearance of the single interface-localized state IF at 2.267 eV. (b) In-plane average density plot of the IF eigenfunction, showing the sharp localization of this state at the InP/GaP interface. Energies are relative to the unstrained GaP VBM (−6.099 eV).

of different symmetry in the bulk can fold into states of either the same or different symmetry in the SL. In the former case, the bulk states will *couple*, leading to changes in the energy position and spatial localization of the resulting SL states as compared to the expected behavior that would follow from a straight folding analysis. Note, however, that the strength of the coupling depends not only on the symmetry, but also on the actual potential of the SL.[11]

This interplay between folding and coupling of folded states is important for understanding the nature of states in both SLs[9,11,13] and, as we show below, QWs. We give in the following the relevant aspects of the BZ folding and states coupling pertaining to common-ion (001) SLs, which are studied here. After clarifying a frequent source of confusion related to X-valley CB states in III–V semiconductors, we discuss the symmetry-governed coupling conditions for two cases that will be encountered in this work: the folding and coupling of (i) X_z and Γ and (ii) X_x and X_y states in (001)-oriented SLs, corresponding to $\vec{n} \parallel Oz$.

A. Geometric folding of states in (001) superlattices

The systems we discuss here are common-ion III–V-based QWs of type $(\mathrm{AB})_n$/AC having (001) orientation ($\vec{n} \parallel Oz$), which can be seen as $(\mathrm{AB})_n/(\mathrm{AC})_m$ SLs with $m \to \infty$. To build the tetragonal supercell used in calculations one needs a number of $(n+m)$ or $(n+m)/2$ zincblende unit cells, depending on whether a face-centered-cubic (fcc) or simple-cubic (sc) unit is used. The corresponding Bravais lattice of the supercell will be simple (body-centered) tetragonal, for $n+m$ even (odd).[13] Following the standard convention we use a bar to denote high-symmetry points in the small BZ of the supercell and consider two cases of folding and states coupling: (i) the bulk CB states at X_z and Γ that fold into $\bar{\Gamma}$ [(0,0,0) in the small BZ] and (ii) the bulk CB states at X_x and X_y folding into $\bar{M}$ [$(2\pi/a$,0,0) in the small BZ]. Case

(ii) occurs for any combination (n,m) while case (i) requires $n+m$ to be even; this further implies that n and m need to have the same parity, being both either even or odd. For $n+m$ odd, X_z folds into the $\bar{Z}$ point, located on the (001) face of the supercell BZ.

B. Symmetry of conduction band X states in zincblende III–V semiconductors

In zincblende III–V semiconductors the two lowest states at the X point of the BZ [coordinates $(2\pi/a,0,0)$] have the atomic orbital representations $X^\alpha =$ (anion-s, cation-p) and $X^\beta =$ (cation-s, anion-p).[14] The order of these two levels depends on the type of anion and cation, in particular on their electronegativities.[15] While in most of III–V compounds X^α is lower than X^β, this order is reversed in BP, GaSb, and InSb.[15]

In bulk, taking the origin on an anion site, the two states are labeled $X_1 = X^\alpha$ and $X_3 = X^\beta$, respectively, being even and odd with respect to symmetry operations that change z into $-z$. A change of the origin to a cation site reverses this symmetry labeling;[16] that is, $X_1 = X^\beta$ and $X_3 = X^\alpha$. This fact has caused much confusion in the literature, often incorrect labels being used, especially in SLs. Indeed, in a common-ion $(AB)_n/AC_m$ SL, the irreducible representations of lower and upper states $X^\alpha =$ (anion-s, cation-p) and $X^\beta =$ (cation-s, anion-p) depend not only on the parity of n, m, and $n+m$, but also on whether the SL is a common anion or common cation.[11,13] For this reason, the symmetry-related coupling rules we list below use the X^α and X^β notation, rather than X_1 and X_3, with the symmetry given *a posteriori*, in terms of the SL point group, depending on each system.

Let us also note here that, for the zincblende structure, the three X points—X_x, X_y, and X_z—in the BZ are equivalent and so any X state is threefold degenerate. This degeneracy is preserved in unstrained SLs, such as GaAs/AlAs or InAs/GaSb, but is lifted in strained systems such as InP/GaP or GaAs/GaP, because, under the biaxial deformation, the energy shift of the X_z and X_x/X_y edges has opposite signs. Since, on the other hand, the folding of bulk wave vectors in supercell wave vectors has purely geometrical reasons, the coupling schemes that are discussed in the following are valid for both strained and unstrained SLs.

C. Coupling of $\bar{\Gamma}$-folded Γ and X_z states

The two bulk states $|\Gamma\rangle$ and $|X_z\rangle$ folding into $\bar{\Gamma}$ point ($n+m$ is even) of the small BZ of the SL will couple only if both have the same irreducible representation at $\bar{\Gamma}$ (point group D_{2d}) with respect to symmetry operations that change z to $-z$.[13] The Γ state is always even in the SL; that is, it transforms as $\bar{\Gamma}_1(\Gamma)$, regardless of n and m parity or the common ion. The irreducible representations of X_z^α and X_z^β, on the other hand, depend on the common ion of the SL (anion or cation), as well as on the n (m) parity.[11,13] For common anion SLs (such as InP/GaP), one has (i) $\bar{\Gamma}_1(X_z^\alpha)$ and $\bar{\Gamma}_4(X_z^\beta)$ for n even and (ii) $\bar{\Gamma}_4(X_z^\alpha)$ and $\bar{\Gamma}_1(X_z^\beta)$ for n odd. In common cation SLs (like GaAs/GaP), the parity dependence is just reversed. As can be seen, X_z^α and X_z^β couple alternatively with Γ, depending on the parity of n. This leads to an oscillatory behavior in n of those eigenstates that result from such a coupling in thin SLs.[9,11] A similar coupling mechanism was observed in the ordered CuAu ($L1_0$) phase of $InGaAs_2$,[17] which is a naturally formed short period, (001)-oriented SL. Calculations have shown that a strong repulsion of Γ and X_z states upon ordering is responsible for the band gap reduction, by lowering the CB minimum (CBM), and for the localization of the CBM state in the GaAs sublattice.[17]

D. Coupling of $\bar{M}$-folded X_x and X_y states

Symmetry-derived arguments govern also the coupling of the $|X_x\rangle$ and $|X_y\rangle$ bulk states folding into the SL $\bar{M}$ point. This represents a symmetry-forced intervalley mixing of exactly degenerate valleys.[11] The two CB states X_{xy}^α and X_{xy}^β (double degenerate in bulk) will have different irreducible representations, depending on the n and m parity and the common ion of the SL.[11,13] For a common anion system, like InP/GaP or GaAs/AlAs, these are (i) $\bar{M}_5(X_{x,y}^\alpha)$ and $\bar{M}_1(X_x^\beta)$, $\bar{M}_2(X_y^\beta)$ for n even and (ii) $\bar{M}_1(X_x^\alpha)$, $\bar{M}_2(X_y^\alpha)$, and $\bar{M}_5(X_{x,y}^\beta)$ for n odd. Since coupling is allowed between states with the same symmetry, it follows that, for n even, the $\bar{M}^\alpha$ states will couple (repelling each other) and the $\bar{M}^\beta$ states remain degenerate, while the opposite happens for n odd. In a common cation SL (such as GaP/GaAs), on the other hand, the selection rules are just reversed.

In addition to this oscillatory character of the X_x-X_y coupling, Dandrea and Zunger[11] have shown that the magnitude of the splitting falls as $1/n$. We find here a similar qualitative behavior also in QW systems when the two coupling bulk states X_x and X_y originate from the well material.

III. METHOD OF CALCULATION

We have calculated the electronic structure of a few (001) $(AC)_n/(BC)_m$ SLs for large m (QW limit) and various combinations of III–V binaries: InP/GaP, GaAs/AlAs, and GaAs/GaP, thus enabling a comparison of common-anion and common-cation combinations as well as the strained versus unstrained situation. Eigenstates were determined using an atomistic pseudopotential plane wave theory applied to strain-minimized atomic positions. For all the systems investigated we have found that the states derived from bulk L valleys are completely delocalized and show no particular behavior. Consequently, they are omitted from the present discussion and we deal only with Γ- and X-derived bulk states.

A. Construction of supercell

We model the well/barrier system using supercells constructed by stacking $5 \times 5 \times (80 + n/2)$ eight-atom cubic unit cells of zincblende structure along the (001) direction. This construction allows both X and L bulk states to fold into the SL BZ. While varying the thickness n of the well, the large thickness of the barrier ($m = 79$ and 80 MLs, respectively, for n odd and even) ensures a full isolation of the QW, necessary to attain a 1-meV convergence of the single-particle eigenvalues, when using periodic boundary conditions for large supercells.

B. Computing the QW eigenstates

The eigenvalues and eigenvectors of the QW system are obtained by solving the single-particle equation

$$\left[-\frac{\beta}{2}\nabla^2 + \sum_{n,\alpha}\widehat{v}_\alpha(\vec{r}-\vec{R}_{n\alpha},\underline{\varepsilon_n}) + \widehat{V}_{\alpha\mathrm{NL}}\right]|\,i\,\rangle = E_i|\,i\,\rangle, \quad (3)$$

where $v_\alpha(\vec{r}-\vec{R}_{n\alpha},\underline{\varepsilon_n})$ is a screened atomic pseudopotential depending on the identity α of the atom and the local strain tensor $\underline{\varepsilon}$ at its relaxed position $\vec{R}_{n\alpha}$:

$$v_\alpha(\vec{r},\underline{\varepsilon}) = v_\alpha(\vec{r},0)[1+\gamma_\alpha \mathrm{Tr}(\underline{\varepsilon})], \quad (4)$$

with γ_α a fitting parameter introducing a further dependence on the identity of the neighbors.[18] The other terms entering Eq. (3) are the nonlocal spin-orbit coupling potential $\widehat{V}_{\alpha\mathrm{NL}}$ and a scaling factor, β, for the kinetic energy.[18]

The unstrained pseudopotentials $v_\alpha(\vec{r},0)$ are determined by requiring that the bulk binaries described by $v_\alpha(\vec{r},0)$ fit experimental and local density approximation (LDA) high-symmetry points (Γ, X, and L) energy eigenvalues and effective masses. Other parameters, such as hydrostatic and biaxial deformation potentials, are extracted during the fitting procedure, but they are merely compared, rather than fitted, to experimental data, and are not explicitly used as such in the supercell calculations. In addition, a fit of the band-gap bowing parameter of the $A_xB_{1-x}C$ alloy is performed for each AB/AC pair of binaries. All the pseudopotential parameters used in this work are given in the Appendix.

Having obtained the pseudopotentials of each atom α and the relaxed positions $\vec{R}_{n\alpha}$, we solve the single-particle equation (3) by making a plane-wave ansatz[19] separately at the $\bar{\Gamma}$ and $\bar{M}$ points of the supercell BZ, calculating all the matrix elements numerically and diagonalizing the Hamiltonian using the folded spectrum method.[20]

C. Lattice relaxation by strain minimization

We obtain the relaxed geometry and configuration of each QW system by minimizing the elastic strain energy. After building the supercell from unrelaxed bulk primitive cells, we simulate the presence of a fixed substrate in the QW geometry by constraining the supercell to preserve its in-plane lattice constant equal to that of the substrate. Along the QW (001) direction, on the other hand, both the supercell height and the atomic positions are allowed to relax around their (bulk) equilibrium values. The elastic strain energy that needs to be minimized is calculated here using the valence force field (VFF) functional in its generalized form:[21–23]

$$\begin{aligned} E &= \sum_i \sum_j^{\mathrm{nn}\,i} \frac{3}{8}\alpha_{ij}\Delta d_{ij}^2 + \sum_i \sum_{k>j}^{\mathrm{nn}\,i} \frac{3\beta_{jik}}{8d_{ij}^0 d_{ik}^0} \\ &\quad \times \left[(\vec{R}_j-\vec{R}_i)\cdot(\vec{R}_k-\vec{R}_i) - \cos\theta_{jik}^0 d_{ij}^0 d_{ik}^0\right]^2 \\ &\quad + \sum_i \sum_{k>j}^{\mathrm{nn}\,i} \frac{3\sigma_{jik}}{d_{ik}^0}\Delta d_{ij} \\ &\quad \times \left[(\vec{R}_j-\vec{R}_i)\cdot(\vec{R}_k-\vec{R}_i) - \cos\theta_{jik}^0 d_{ij}^0 d_{ik}^0\right]. \end{aligned} \quad (5)$$

In this equation, $\Delta d_{ij} = [(\vec{R}_i-\vec{R}_j)^2 - (d_{ij}^0)^2]/d_{ij}^0$, $\vec{R}_i$ is the coordinate of atom i, and d_{ij}^0 is the ideal (unrelaxed) bond distance between atoms i and j. Further, θ_{jik}^0 is the ideal (unrelaxed) angle of the bond j–i–k. The notation $\sum^{\mathrm{nn}\,i}$ denotes summation over the nearest neighbors of atom i. The bond stretching, bond angle bending, and bond-length/bond-angle interaction terms are described by the VFF parameters $\alpha_{ij}, \beta_{ijk}, \sigma_{ijk}$, which are related to the elastic coefficients C_{ij} of the corresponding bulk material.[23] For the present calculations, we have used for InP, GaP, and GaAs the parameters listed in Ref. 24, whereas for GaAs/AlAs we considered a zero lattice mismatch and thus no further relaxation of the corresponding QW system.

D. Eigenstates postprocessing: Bloch character and interband absorption

A plane-wave expansion for the eigenfunctions of Eq. (3) also enables us to analyze the bulk Bloch character preserved in each of the numerically determined solutions. Indeed, while Eq. (1) describes the folding of Bloch states into SL states, the reverse operation, unfolding of an SL state into its Bloch components is also possible and relatively straightforward,[12,25] being accomplished by simply projecting the eigenfunctions $|\,i\,\rangle$ of Eq. (3) on Bloch waves $|\,\vec{k},\mu\rangle$ of the SL parent unit cell.

We have also calculated the optical absorption spectrum $I_{vc}(E)$, taking VB $\rightarrow$ CB (interband) transitions within the dipole approximation. Denoting the matrix element of this transition by $M_{vc} = \langle\, v|\,\widehat{p}\,|\,c\rangle$, the absorption spectrum is

$$I_{vc}(E) \propto \sum_v \sum_c |M_{vc}|^2 \delta(E_c - E_v - E), \quad (6)$$

with $E = \hbar\omega$ the energy of the absorbed photon.

IV. ORIGIN OF INTERFACE-LOCALIZED STATES

In this section, we present results of atomistic pseudopotential calculations meant to mimic a single InP/GaP interface on a GaP(001) substrate, corresponding to half-infinite GaP/GaP(001) on one side and half-infinite InP/GaP(001) on the other side, as depicted in Fig. 3, which also shows the band offsets across the InP/GaP/GaP(001) heterojunction. We note that these are actually calculated band edges of the corresponding binaries and, as such, the resulting confining potentials shown here have only an illustration purpose. The energy reference is taken as the unstrained GaP valence band maximum (VBM) at −6.096 eV. For our following analysis, the X_{xy} CB states are of no interest and have been omitted from this figure. It can be seen that this junction has a type II CB offset, with a direct-gap material on one side and an indirect gap material on the other, the Γ and X_z profiles being interlaced. We discuss and analyze the single IFLS—labeled IF in Fig. 3—emerging at the InP/GaP interface as a result of this particular offset and its evolution into a pair of IFLSs when forming the QW.

A. Models of interface states in a single heterojunction

Early attempts on theoretical predictions of surface and interface states date to the 1930s, when Tamm[26] and Shockley[27] first showed that the abrupt termination of a periodic one-dimensional potential with a barrier leads to the appearance of new solutions, characterized by a complex wave vector, and thus decaying exponentially into the barrier. These states were found to be energetically positioned either in the allowed or forbidden energy bands of the unperturbed potential. While both of these works considered the potential termination as characteristic to a surface, thus describing a vacuum interface, James[28] applied the more general transfer matrix method to show that any finite perturbation to a periodic potential introduces new, localized states that can be either in the energy bands or in the gaps.

The case of intervalley coupling in one dimension was treated by Trzeciakowski,[29] who employed the same transfer matrix method of James.[28] In his model, Trzeciakowski made no assumptions about the form of the potential, other than it is periodic on both sides of the interface between two materials A and B. He arrived at two different cases for the occurrence of IFLSs: (i) inverted-band systems, that is, the CB in material A matching the VB in material B, thus recovering the effective-mass-based results;[7,8] (ii) similar bands (conduction or valence) meeting at the interface, that is, without a change in sign of the effective mass, but of different type (symmetry), for example, Γ and X. This led to the conclusion that IFLSs might be possible at the GaAs/AlAs or Si/Ge interfaces.[29]

B. Appearance of a single interface state at the InP/GaP junction

To obtain the eigenstates for the single heterojunction InP/GaP/GaP(001) we apply the approach described in Sec. III, considering an $(\mathrm{InP})_n/(\mathrm{GaP})_m$ SL with $n = m = 80$ MLs. Such large n and m values ensure (i) a complete separation of the two InP/GaP interfaces and (ii) the suppression of any confinement effects. Since we are dealing with a (001)-oriented quasi-two-dimensional system, we expect that the SL states, solutions of the single-particle Eq. (3) of wave vector $\vec{K} \equiv \bar{\Gamma}$, to be linear combinations of all the Bloch states of wave vector $\vec{k}_i = (0,0,z_i)2\pi/a$, with $z_i = (i-1)/(n+m)$, $i = 1,\ldots,(n+m)$. This follows directly from Eqs. (1) and (2), in the particular case of $\vec{n} \parallel Oz$ and $n+m = 160$. In other words,

$$|\bar{\Gamma}\rangle = \sum_{i}^{n+m} A(\vec{k}_i;\bar{\Gamma})|\vec{k}_i\rangle = A(\Gamma;\bar{\Gamma})|\Gamma\rangle + A(X_z;\bar{\Gamma})|X_z\rangle + \sum_{1<i<n+m} A(\vec{k}_i;\bar{\Gamma})|\vec{k}_i\rangle. \quad (7)$$

We have already mentioned in Sec. III that assuming such a linear combination of Bloch waves to hold allows one to determine the amount of Γ, X_z, or any other wave vector of the parent lattice preserved in the actually calculated SL eigenstate $|\bar{\Gamma}\rangle$. We are interested in the SL eigenstates in the energy range between the strained Γ CB edge of InP and the unstrained X_z CB edge of GaP. Except for two states, which are designated in the following by IF, all the other solutions in this energy range proved to be extended states. The two states standing out as exceptions were found at $E_{\mathrm{IF}} = 2.267$ eV, separated by less than 1 meV, and were identified as IFLSs. As shown in the bottom panel of Fig. 3, they are characterized by a sharp interface localization, on the GaP side of the heterojunction, extending over about 4 MLs. A spectral analysis of these states showed that they consist of *only* the first two terms in Eq. (7), in equal parts, in other words, the IFLSs have exclusively Γ and X_z character.

Our interpretation of this result is the following. At the single heterojunction formed between strained InP and GaP there is a single IFLS present, at E_{IF}, made of only Γ and X_z Bloch waves. The direct calculation showing two such states nearly degenerate is related to the second interface, decoupled from the first one, present *de facto* in the SL system. As seen in Fig. 3, in terms of electron wave packets moving toward the interface, we will have a Γ repulsion for InP-based waves, but the simultaneous presence of an X_z repulsion *and* a Γ attraction for GaP-based waves. The two Bloch wave functions Γ and X_z are very different at the interface because one vanishes and the other does not. If, as a result of the coupling, the part of the admixture is transferred to the vanishing wave function, the two Bloch waves can be matched. As pointed out by Trzeciakowski,[29] such a matching is possible only when the energy difference is large enough (but not too large as to decouple the two states completely).

We note here that the situation we encountered for the InP/GaP interface corresponds to the second case proposed by Trzeciakowski,[29] that of a heterojunction between two materials with different CB minima, one Γ and one X. In contrast to the one-dimensional model, however, the energy E_{IF} of the interface state lies between the CBM values in the two materials, $E_\Gamma = 2.074$ eV and $E_X = 2.363$ eV. Such a positioning of the IFLS, between the band edges across the junction, was predicted for inverted band systems, like HgTe/CdTe,[7,8] where the effective mass changes its sign from one side of the junction to the other.

We conclude that a generally valid mechanism can be used to describe IFLSs appearing naturally from CB states at the heterojunction of two semiconductors. Such states shall appear whenever (i) the two materials A and B forming the heterojunction have interlacing bulk band edges that (ii) fold into the *same* point of the two-dimensional BZ, where they are symmetry-allowed to couple. An example is the one at hand, Γ and X_z edges, with Γ and X_z bulk BZ points folding into $\bar{\Gamma}$. We describe in the next section how, by coupling two interfaces, the two isolated IFLSs evolve into a pair in a QW system.

C. Modeling two interacting interface states

Forming the QW is equivalent to having two single junctions, as depicted in Fig. 4, each of them with its own single IF state as calculated in the previous section. For thick QWs, the two single IFLSs will be independent one from another but, as the thickness of the QW decreases, thus bringing the single junctions closer, the two states will start to couple, giving rise to a bonding-antibonding (symmetric-antisymmetric) pair,

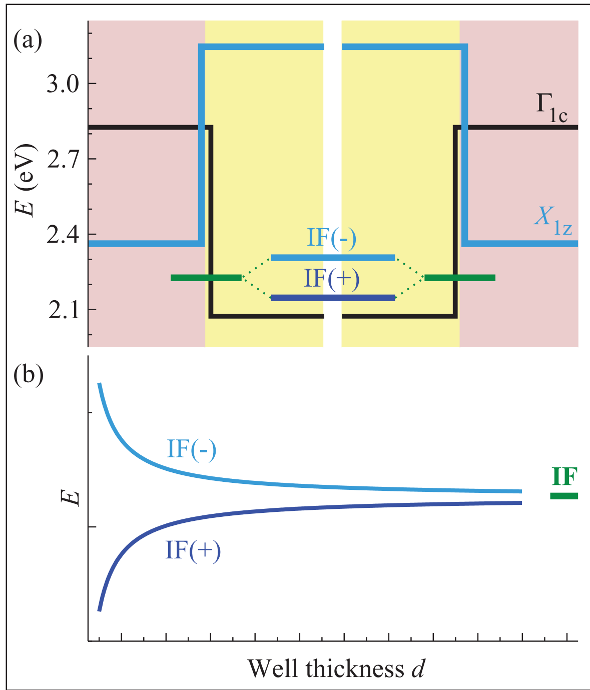

FIG. 4. (Color online) InP/GaP QW epitaxially strained to GaP(001) formed between two heterojunctions. (a) Calculated CB offsets between the Γ and X_z valleys leading to the appearance of the single interface-localized state IF at 2.267 eV for the isolated heterojunctions. (b) Modeled evolution of two single IFLSs into a bonding-antibonding (symmetric-antisymmetric) pair IF(+)/IF(−), when the formation of a QW of thickness d is simulated by bringing two isolated InP/GaP interfaces closer together. Energies are relative to the unstrained GaP VBM (−6.099 eV).

denoted by IF(+) and IF(−).[7] Such an interaction can be described by a two-level interaction model:

$$E_{\pm} = \frac{E_1 + E_2}{2} \pm \sqrt{\left(\frac{E_1 - E_2}{2}\right)^2 + U^2}. \tag{8}$$

Taking $E_1 = E_2 = E_{\mathrm{IF}}$ and an explicit separation dependence of the two-level coupling, $U = U_0/d$, this simply reduces to

$$E_{\pm} = E_{\mathrm{IF}} \pm U_0/d. \tag{9}$$

A qualitative representation of this model is plotted in the bottom panel of Fig. 4. As can be seen, the two-level interaction predicts the existence of two IFLSs in QWs, with an energy splitting that increases with decreasing QW thickness.

We show that these predictions are only partially fulfilled in a realistic system like the InP/GaP QW. Indeed, the symmetric component can further couple to a QW-localized state (a separate bound state created by the Γ well) with compatible symmetry. As a result of the interplay between the Γ-well attraction combined with the X_z repulsion, this new formed state will possess both QW and interface localization. In addition, in the range of thin QWs, the finite size effects become important, and the two interface states IF(−) and IF(+) remain more or less close, instead of diverging.

V. ELECTRON STATES IN INP/GAP QW: STRONG INTERFACE-LOCALIZED STATES FORM THE CONDUCTION BAND MINIMUM

Amongst the large number of calculated CB (electron) eigenstates of the $(\mathrm{InP})_n$/GaP QW, we focus on few of those which are singled out because of their particular spatial localization or energetic position. Their evolution with the well thickness n can be followed in Fig. 5(a), while representative wave function plots are depicted in Fig. 1. We also show, in Fig. 5(b), the CB offsets between the unstrained GaP and the epitaxially strained InP on GaP(001) meant as guidance for the electron confinement in the $(\mathrm{InP})_n$/GaP QW system. The energy zero is taken to be the unstrained GaP VBM.

The Γ well (black solid line) formed by inserting InP into GaP is ∼0.75 eV deep but is resonant with the GaP X continuum. Since InP is biaxially strained to the GaP(001) (lattice misfit ≃7%), its X valleys degeneracy is lifted, forming the two levels X_z and X_{xy} which have opposite shifts under biaxial strain. This leads to the formation of a potential well [X_{xy} valleys, red (dark gray)] and an antiwell [X_z valleys, blue (light gray)] along the GaP/InP/GaP QW. The latter have a height of ≃1 eV. We distinguish the following electron states:

States confined by the Γ well (black well and symbols in Fig. 5). This is the state labeled as $e_s(\Gamma)$ in Fig. 1. For thick QWs ($n \geqslant 8$), its energy is below the CBM of the GaP matrix; i.e., it is a localized gap state. It remains, however, above IF_1 and IF_2 up to $n = 11$. As the QW thickness decreases,

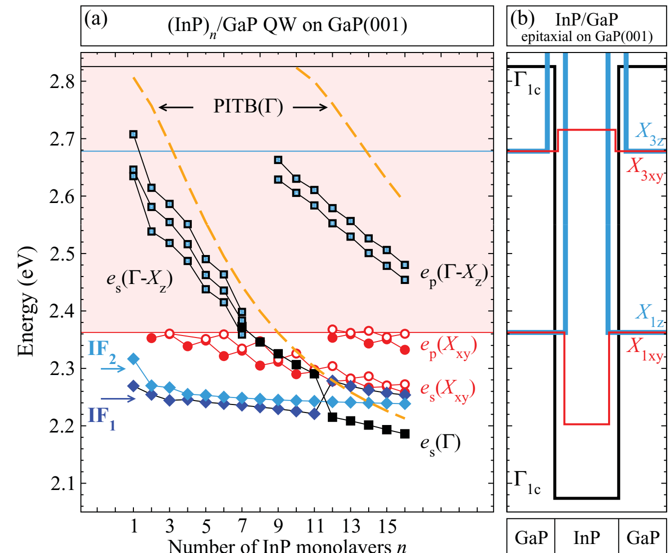

FIG. 5. (Color online) (a) Calculated electron energy levels for the $(\mathrm{InP})_n$/GaP QW system. Delocalized states found within the matrix CB continuum (shaded background) are not shown. The labels designate different states as described in Fig. 1. In addition, analytical results obtained using the particle-in-the-box model (PITB) for the Γ-confined states are shown by dashed lines. (b) The InP/GaP CB offset of Γ, X_1, and X_3 valleys for InP epitaxially on GaP(001). All energies are relative to the unstrained GaP VBM (−6.099 eV).

the energy of $e_s(\Gamma)$ increases monotonically until it becomes resonant with the GaP matrix continuum [shown as a shaded background in Fig. 5(a)] at $n = 7$ MLs. The discontinuity in the n dependence of $e_s(\Gamma)$ is due to its coupling with one of the IFLSs, and it is discussed in more detail below.

It is interesting, at this point, to compare the results of the direct calculation with those obtained using a particle-in-the-box (PITB) model, shown as dashed lines in Fig. 5(a). These were obtained using a unique potential well (of depth 0.75 eV) formed by the Γ valleys, the effective mass of Γ electrons in InP, and ignoring any intervalley coupling. The PITB model predicts two bound states in the Γ well, the first one existing already for $n = 1$ ML, the second appearing at $n = 10$ MLs. Comparison with the numerical results allows us to identify the first solution as being the gap-localized $e_s(\Gamma)$ state for $n \geqslant 8$ MLs. In addition, when the Γ-confined states are resonant with the continuum—that is, $n \leqslant 7$ MLs for the first solution and all n values for the second—a special case of the coupling discussed above (Sec. II) occurs: bulk states of wave vectors $\vec{k} = (0,0,k_z)$ that fold into $\bar{\Gamma}$ [compare with Eq. (7)] may couple to the resonant $e_s(\Gamma)$ or $e_p(\Gamma)$ states. This leads to the appearance of the hybrid states $e_s(\Gamma - X_z)$ and $e_p(\Gamma - X_z)$, denoted by open squares in Fig. 5(a). It is obvious that the hybrid states $e_s(\Gamma - X_z)$ show up as a continuation, below $n = 7$ MLs, of the Γ-well confined $e_s(\Gamma)$ state. Wave-function plots of $e_s(\Gamma - X_z)$ are shown in Fig. 1 for $n = 1$ and $n = 2$ MLs. They are characterized by a large ($\simeq$13%) bulk Γ character and possess a fingerprint of interface localization overlapped with a delocalized background. In the absence of the $e_s(\Gamma)$ or $e_p(\Gamma)$ resonances, these $(0,0,k_z)$ states, expelled by the X_z antiwell, would be extended in the GaP barrier.

This shows that the confinement of Γ electrons manifests itself also in those energy regions where the confined states are resonant with the continuum. As long as extended states with compatible symmetry are present (in this case, along the Γ-X_z bulk BZ direction), the resonant confined states may couple with them, generating hybrid states that can open strong optical transition channels (see below). It is also noteworthy to mention that, in addition to the deep, isolated single IF state appearing at the single InP/GaP heterojunction (Sec. IV B) the same mechanism is present in the continuum: weakly localized IF states are evidenced in our results for InP/GaP QWs.

States confined by the X_{xy} well [*red (dark gray) well and symbols in Fig.* 5]. Because of the different offsets of the X_1 and X_3 edges between InP and GaP, only the strained X_1 valley forms a well. This leads to the QW localization of X_{xy} electrons, an example being shown in the rightmost panel of Fig. 1. These InP-localized states at $\bar{M}$ follow the expected behavior discussed in Sec. II D for the lower ($X^\alpha \equiv X_1$) state in a common anion system. As seen in Fig. 5(a), there are two sets of X_{xy}-confined levels, appearing in pairs: $e_s(X_{xy})$, present for $n \geqslant 2$ MLs, and $e_p(X_{xy})$, appearing for thicker QWs, at $n \geqslant 12$ MLs. Their splitting shows an oscillatory magnitude, whereas it is negligible for n odd, it is finite and decays as $1/n$ for n even.

Interface-localized states IF_1 and IF_2. As we have seen above, under the band edge mismatch $(\Gamma - X_z)$ and offset conditions described above (Sec. IV B) an IFLS appears at each GaP/InP heterojunction. In the limit of very thick QWs, the system will have two independent IFLSs, at approximately the same energy. We note here that, within an atomistic modeling, the two interfaces are never perfectly identical since the zincblende structure lacks the inversion symmetry. As the thickness of the QW is reduced, a simple two-level interaction model—see Eq. (9) and Fig. 4—could be used to describe the coupling of the two states leading to the formation of a bonding-antibonding pair, with a splitting between them that will increase with decreasing QW thickness.

Our calculations for the $(InP)_n/GaP$ QWs reveal the existence of these two IFLSs, labeled IF_1 and IF_2 in Fig. 1, where their in-plane averaged density shows a sharp localization, extending over ~4 MLs at the InP/GaP interface, a similar range as the one obtained for the single interface case shown in Fig. 3. The spectral analysis of the IFLSs confirmed that they preserve, even for thin QWs, a nonzero Γ character. Its specific values at selected thickness n are given below the corresponding energy values of IF_1 and IF_2 in the right corner of each panel of Fig. 1.

It can be seen from the n-dependence of both IF_1 and IF_2 [Fig. 5(a)] that the IFLSs form the CBM of thin $(InP)_n/GaP$ QWs. In the following, we investigate in more detail this dependence and how it differs from the two-level interaction model. For this reason, Fig. 6 shows the two IFLSs on an enlarged energy scale, together with the Γ-well confined state $e_s(\Gamma)$. Two distinct regions are of interest, that of ultrathin QWs, $n \leqslant 5$, and that of IF_1-$e_s(\Gamma)$ coupling, for $n \geqslant 9$.

In the first region, at small n values, the two IFLSs IF_1 and IF_2 have the same slope with decreasing n, instead of diverging, as the simple model predicted. Their splitting shows an alternating magnitude. This indicates a parity-dependent coupling (odd or even n), similar to the one discussed above for thin SLs. The missing divergent character of the two branches is a direct consequence of the finite size effect of the QWs captured by the atomistic approach but missed by the model. Indeed, as the QW thickness is comparable with the IF_1 and IF_2 localization range, the two IFLSs can no longer be treated as independent, and thus their repulsion will be weaker.

The single interface state shown in Fig. 3 represents the asymptotic limit of IF_1 and IF_2. The antisymmetric IFLS IF_2 shows a monotonous convergence toward $E_{IF} = 2.267$ eV.

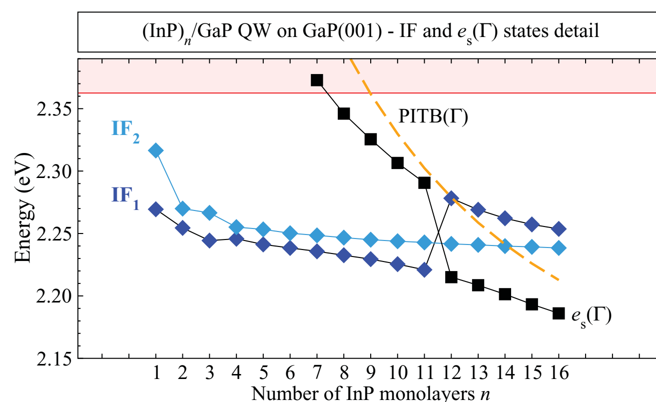

FIG. 6. (Color online) Calculated electron energy levels for the $(InP)_n/GaP$ QW system showing details on the interface (IF) and Γ-confined $e_s(\Gamma)$ states of Fig. 5.

Furthermore, as n increases, the amplitude of the interface peaks and the amount of IF_2 Γ character show no dependence on n. In contrast, the symmetric IF_1 state has a discontinuity in its n dependence, that coincides with a similar behavior of $e_s(\Gamma)$. Because both IF_1 and $e_s(\Gamma)$ are symmetric, they are allowed to couple. This is, of course, an additional coupling to the one that generated the symmetric-antisymmetric pair, IF_1 and IF_2. As $e_s(\Gamma)$ plunges into the matrix gap, the increased confinement bringing it closer to IF_1, this coupling gains in strength. A significant transfer occurs, from $e_s(\Gamma)$ to IF_1, of Γ character and QW localization, as can be seen in Fig. 1. At $n = 12$ MLs, the Γ-well confinement is strong enough to bring $e_s(\Gamma)$ below both IFLSs. The mutual repulsion of $e_s(\Gamma)$ and IF_1 is still present, but now, with increasing QW thickness n, it becomes weaker and the two states regain their identity of QW-localized and IFLS, respectively. This complex mechanism of states coupling can have important consequences on the optical and transport properties of such systems.

VI. STRONG ABSORPTION DUE TO INTERFACE STATES IN INP/GAP

A. The InP/GaP QW system

Interband absorption spectra for thin $(\mathrm{InP})_n/\mathrm{GaP}$ QWs, with $n = 1, \ldots, 4$ were calculated using the highest 40 hole and the lowest 60 electron states of each system, according to Eq. (6). The spectra, shown in Fig. 2, were subsequently broadened using an energy-independent Gaussian of FWHM of 4 meV.

The low-energy part of the absorption spectra exhibit sharp peaks stemming from transitions from the two highest QW-confined hole states (h_0 and h_1) into the IF_1 and IF_2 states. For $n = 1$ ML, these correspond to 2.17 eV ($h_0 \mapsto IF_1$), 2.21 eV ($h_1 \mapsto IF_1$ and $h_0 \mapsto IF_2$), and 2.24 eV ($h_1 \mapsto IF_2$). These values are in excellent agreement with the ultrathin InP/GaP QW PL measurements of Hatami *et al.*[10] For thicker QWs ($n = 3$ and $n = 4$) a change in the relative amplitudes of the IF_1- and IF_2-related absorption lines can be observed. This is a direct consequence of the parity-dependent coupling of IF_1 and IF_2 at small n values discussed above.

The $h_{0,1} \mapsto IF_{1,2}$ lines redshift with increasing QW thickness, a shift observed also experimentally. Its main origin is the upward shift in energy of the initial states, the QW-confined hole states h_0 and h_1 (not shown), as the QW becomes thicker. Indeed, as can be seen from Fig. 6, the lowering of IF_1 between $n = 2$ and $n = 4$ MLs is less than 10 meV, which is one order of magnitude smaller than the corresponding redshift of its absorption peak.

Above the IF_1- and IF_2-related transitions, we observe an increased contribution involving the extended and matrix-resonant electron states $e_s(\Gamma - X_z)$. The latter, which are indirect in real space (QW to matrix), stand out because of their increased oscillator strength, a signature of their large Γ character. Thus, these transitions are direct in reciprocal space and hence strong. Because their initial states are QW-confined states, these peaks show a redshift similar in magnitude to that of the IF-related transitions.

Time-resolved PL measurements on InP/GaP QWs of Hatami *et al.*[10] have shown that the QW transitions have a long decay time of $\simeq$19 ns. Such long lifetimes, characteristic to type II transitions, as well as the effective mass modeling of the authors, which gave (in agreement with our pseudopotential calculations) no confined Γ state for thin QWs, had led to the conclusion that the PL in these systems comes from type II transitions in both real and reciprocal space. Our results, consistent with the experimental findings, suggest that the lowest transitions involve IFLSs: their spatial localization gives the transitions an indirect character, while their large Γ character provides an increased oscillator strength as compared to pure X states.

B. Do the interface states appear in InP/GaP quantum dots?

Despite the similar lattice mismatch to InAs/GaAs ($\simeq$7%), the growth of InP/GaP QWs or quantum dots (QDs) on GaP(001) substrate is much more difficult. Optical properties of InP/GaP QDs grown on GaP(001) were reported, amongst others, by Hatami *et al.*[30–33] and Goñi *et al.*[34] In all these experiments, a crucial difference has been emphasized between the behavior of QDs and QWs: While PL transitions in InP/GaP QWs are indirect in both real and reciprocal space, they become direct in both spaces in InP/GaP QDs. High-pressure measurements[34] evidenced a type I to type II transition in the PL: The slope of PL-pressure dependence changes sign at $\sim$0.15 GPa, thus supporting an intradot type I PL transition below this threshold. We suggest, however, that our present results for InP/GaP QWs are consistent with both findings, in QWs and QDs, providing a unified interpretation of the experimental results based on the occurrence of the IFLSs.

Indeed, in a QD system, $\vec{k}$ is no longer a good quantum number. As such, the QD states are the result of the folding of all $\vec{k}$ points of the bulk BZ. Specific to the IFLSs discussed above, one may obtain three times more IF states, since not only X_z [as it is the case for a (001)-QW], but also X_x and X_y valleys will fold together. Such IFLSs may localize above, below, and even on the lateral sides of the QD, as found by Williamson *et al.*[35] for spherical InP QDs subjected to hydrostatic compression.

The confinement in wide dots mainly occurs along their growth direction $\vec{n}$ and it is thus reasonably described theoretically by thick QWs. As seen in Fig. 1 for $n = 10$, which corresponds to an InP QW thickness of $\sim$3 nm, the lowest state, resulting from the $e_s(\Gamma)$-IF_1 coupling, has a large Γ character ($\simeq$24%) and QW localization, both accounting for a strong, pseudo-type-I transition. As observed by Goñi *et al.*[34] an increased pressure will produce an upward shift of the Γ valley, which will have two consequences: (i) the $\Gamma - X_z$ offset and (ii) the depth of the Γ well will both be reduced. Both effects concur to the disappearance of the IFLSs, and the PL transitions related to them will smoothly evolve from pseudo-type-I to type II. In contrast, an increased pressure lowers the X_{xy} valley, such that the X_{xy} well gets deeper, and the InP-localized $e_s(X_{xy})$ states become the lowest electron levels of the QD system. In this case, at high-enough pressure, the PL transition is indirect in reciprocal space but remains direct (intradot) in real space.

VII. OTHER III–V SYSTEMS WITH INTERLACING $\Gamma - X_z$ OFFSETS

A. InP/GaP QW system on GaAs(001): Interface states still present

The large lattice mismatch between InP and GaP creates a considerable biaxial strain that leads, as we could see, to a large X_z-X_{xy} splitting within the InP QW. Instead of this extreme situation—which is also the cause for InP/GaP on GaP(001) QWs not being easily grown—we can simulate the epitaxial growth of InP/GaP on GaAs(001). Since GaAs lattice constant is approximately midway between InP and GaP, this corresponds to a smaller (∼4%) compressive strain of InP accompanied by a similar tensile strain of GaP. As a result, the X_z-X_{xy} splitting will occur in both materials, leading to the strained CB offset shown in the left panel of Fig. 7. Such a modified offset may also occur if—as a result of misfit dislocations—the InP/GaP QW would not be totally pseudomorphic to the GaP(001) substrate.

Comparing the two systems with different substrates shows that (i) as a result of the tensile strain, both Γ and X_z edges of GaP are shifted downward in energy as compared to the unstrained situation, while the X_{xy} edge is shifted upward; (ii) the reduced compressive strain of InP results in a lower energetic position of its Γ and X_z edges, whereas the X_{xy} edge is higher. As a consequence, the Γ and X_{xy} wells are shallower in InP/GaP/GaAs(001) than in InP/GaP/GaP(001), and the height of the X_z antiwell is smaller. The Γ well and the X_z antiwell, however, remain interlaced.

We also compare, in the middle panel of Fig. 7, the three lowest electron states calculated for a 5-ML-thick InP QW embedded in the same GaP barrier but on different substrates, GaAs(001) (left) and GaP(001) (right). We find that the IFLSs are still present even in the case of a reduced Γ-well depth and X_z antiwell height. The IFLSs in InP/GaP/GaAs(001) appear at a lower energy than in InP/GaP/GaP(001), not only on the absolute scale, but also relative to the barrier $X_z$edge. This is in line with our expectations formulated above for single interfaces: the larger the $\Gamma - X_z$ mismatch, the deeper the IFLS.

The changes in the CB offsets have important consequences also for the position and nature of the lowest QW-localized level. The X_{xy} well is deeper for GaAs(001) substrate and a QW-confined $e_s(X_{xy})$ pair still exists (not shown). However, the Γ well is now positioned low enough in energy to allow the $e_s(\Gamma)$ state—the electron confined by the Γ well—to appear below both $e_s(X_{xy})$ and the barrier continuum onset.

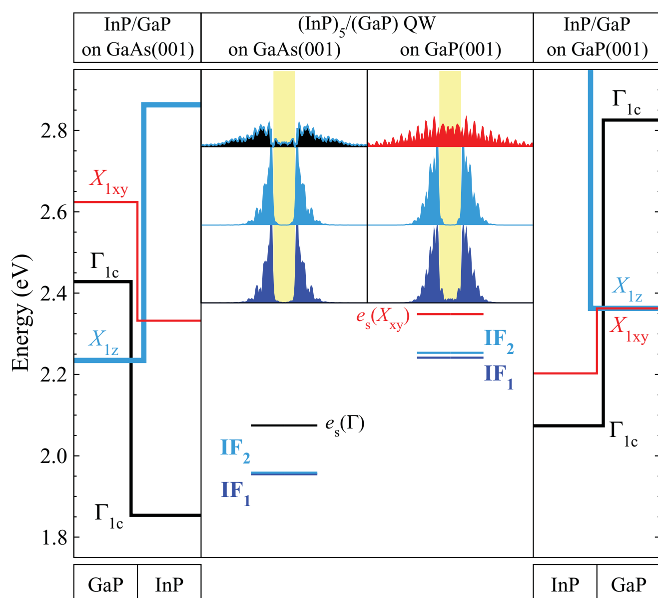

FIG. 7. (Color online) Comparison of the InP/GaP CB offset and the lowest three electron states in the $(InP)_5$/GaP QW system for two different substrates: GaAs(001) (left) and GaP(001) (right). In the former case, both InP and GaP are subject to biaxial strain which leads to X_z-X_{xy} splitting in both materials.

B. GaAs/AlAs QW system: Weak interface states in the continuum

The GaAs/AlAs QW system is analogous to InP/GaP in its being a common cation system and thus subject to similar Γ-X_z and X_x-X_y coupling selection rules. However, GaAs and AlAs are nearly perfectly lattice matched, so there is no strain in this structure that might modify their natural band offset. Thus, no strain-induced splitting between X_{xy} and X_z occurs. As shown in Fig. 8(b) (energy reference is the AlAs VBM at −6.004 eV), while a Γ well is present in GaAs/AlAs QWs, both X_{xy} and X_z form an antiwell, of height ∼0.3 eV. The first obvious consequence is the absence of any X_{xy}-localized states. Results of calculations performed for GaAs QWs of varying thickness n are illustrated in Fig. 8(a) (electron energy levels) and Fig. 9 (in-plane averaged density plots). We find the following states:

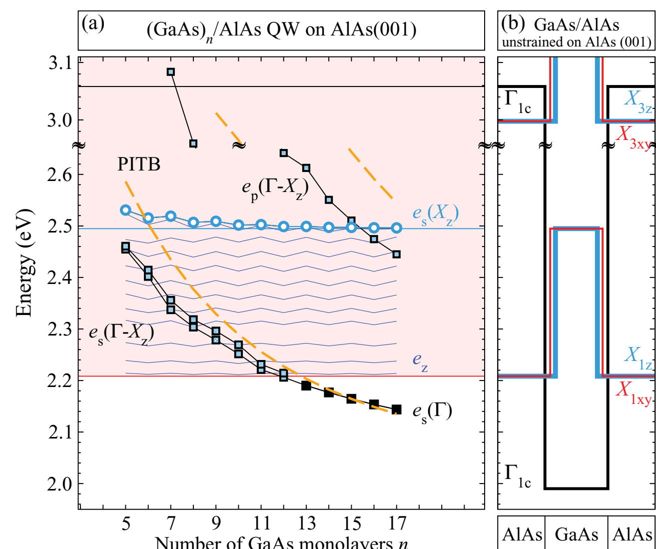

FIG. 8. (Color online) (a) Calculated electron energy levels for the $(GaAs)_n$/AlAs QW system. Delocalized states found within the matrix CB continuum (shaded background) are not shown. The labels designate different states as described in the text. In addition, analytical results obtained using the PITB model for the Γ-confined states are shown by dashed lines. (b) The GaAs/AlAs CB offset of Γ, X_1, and X_3 valleys unstrained (lattice matched) on AlAs(001). All energies are relative to the unstrained AlAs VBM (−6.004 eV).

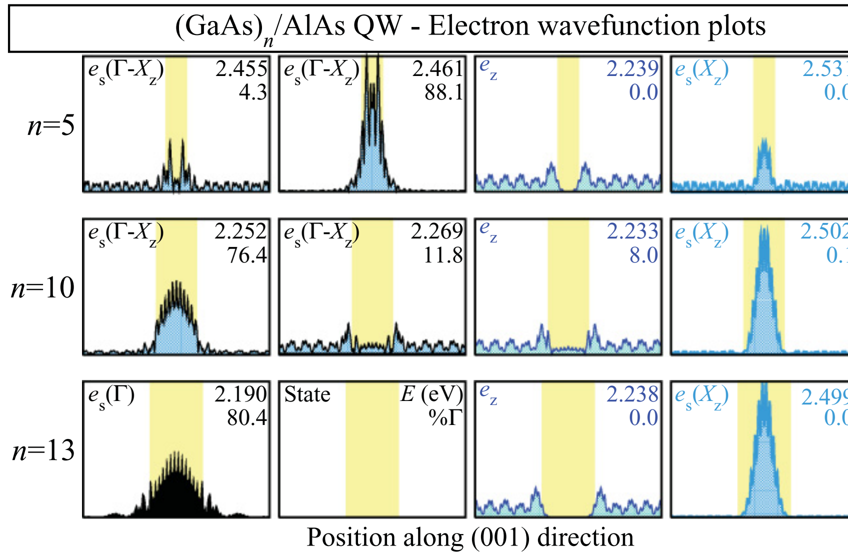

FIG. 9. (Color online) In-plane average density of selected electron wave functions along the (001) growth direction in $(GaAs)_n(AlAs)$ QW system, calculated for different numbers of ML n. From top to the bottom, $n = 5$, 10, and 13 MLs, respectively. The yellow (light gray) shaded area marks the position of the GaAs QW. The numbers in the top right corner of each panel indicate the energy of the corresponding state (in eV, relative to AlAs VBM) and its amount of Γ character. Only the $e_0(\Gamma)$ state at $n = 13$ lies below the AlAs CBM (2.194 eV).

States confined by the Γ *well* (*black well and symbols in Fig.* 8). We find $e_s(\Gamma)$ states below the matrix (AlAs) CBM for thick QWs, $n \geqslant 13$ MLs GaAs. For thinner wells, $e_s(\Gamma)$ is in resonance with the matrix CB continuum. A second Γ state, $e_p(\Gamma)$, remains AlAs CB resonant even for thick values of n. Comparing the direct calculation with the PITB model (dashed lines in Fig. 8) shows that, in contrast to InP/GaP QW, the effective mass approximation predictions lie much closer to the actual pseudopotential results. Important for our discussion is to note that also the dependence of $e_s(\Gamma)$ on n is fairly similar in the two calculations, a consequence of the missing interacting (symmetric) IFLS below $e_s(\Gamma)$.

As can be seen in Fig. 9 for $n = 5$ and $n = 10$ MLs, the resonant $e_s(\Gamma)$ couples to various bulk states of $(0,0,k_z)$ vectors that fold into $\bar{\Gamma}$, leading to the hybrid states $e_s(\Gamma - X_z)$ [and the complementary $e_p(\Gamma - X_z)$], denoted by open squares in Fig. 8. This is a similar behavior to the one observed for InP/GaP QWs above.

States confined by the X_{xy} *well*. Since no X_{xy} well is present, no such states exist in GaAs/AlAs.

X_z*-localized states* [*open blue (light gray) symbols in Fig.* 8]. An interesting case of a resonant state is the $e_s(X_z)$ state depicted in the rightmost panel of Fig. 9. This state is characterized by a strong GaAs (QW) localization, independent on its thickness, and its Γ character is zero. As can be seen in Fig. 8(a) (open symbols), $e_s(X_z)$ is located slightly above the GaAs X_{1z} edge with its energy showing a weak, oscillating variation with the QW thickness n. The occurrence of this state is the result of a symmetry-imposed mixing of two degenerate bulk states that segregate in two different regions of a heterojunction, as has been discussed by Wei and Zunger.[9]

Natural IFLSs: where are they? There are no deep IFLSs in the barrier gap, as present in InP/GaP QW. Instead, we found several states, labeled e_z in Fig. 8(a) (thin lines), that are partially extended in the barrier and have a small degree of localization at the GaAs/AlAs interface, as shown by the e_z state depicted in Fig. 9. The smaller height of the X_z antiwell and the reduced $\Gamma - X_z$ offset (0.2 eV) make these states to remain resonant in the continuum, instead of being pushed into the gap. Let us note, however, that their existence, in the absence of strain, fully justifies their designation as "natural" IFLSs, originating solely from the potential variation across the heterojunction. These states are characterized by a very small Γ character. However, they are symmetry-compatible and may couple with $e_s(\Gamma)$ when the energy separation between the two states is small. As shown in Fig. 9 for $n = 10$ MLs, where the e_z-$e_s(\Gamma - X_z)$ separation is ∼20 meV, the e_z acts as resonator to $e_s(\Gamma)$, borrowing from it Γ character and well localization.

C. GaAs/GaP QW system: Interface states in the continuum

The two previous systems were common anion; we discuss now GaAs/GaP, a common cation QW. We chose the same GaP(001) substrate, such that this system differs from InP/GaP QW only in the QW material and its associated biaxial strain. The lattice misfit between GaAs and GaP is only ∼3.5%, as compared to ∼7% in InP/GaP. The resulting biaxial strain, however, is still big enough to cause the appearance of an X_{xy} well and X_z antiwell, as seen in Fig. 10(b), where the CB offsets between the GaAs strained Γ and X valleys are shown relative to those of the unstrained GaP barrier. The reference energy is the GaP VBM (−6.096 eV).

States confined by the Γ *well* (*black well and symbols in Fig.* 10). The depth of the Γ well (the difference between the strained GaAs and unstrained GaP Γ edges) is ≃0.57 eV, and thus smaller than in the previous two systems. Not surprisingly, although the effective mass of GaAs is slightly larger than that of InP, the $e_s(\Gamma)$ state in GaAs/GaP QWs falls below the GaP CBM only for $n \geqslant 16$ MLs GaAs. Below this thickness it remains resonant with the GaP continuum, giving rise to the weakly coupled $e_s(\Gamma - X_z)$ states [open squares in Fig. 10(a)], seen already for InP/GaP and GaAs/AlAs QWs.

States confined by the X_{xy} *well* [*red (dark gray) well and symbols in Fig.* 10]. The CBM of the $(GaAs)_n$/GaP QW is formed by the $e_s(X_{xy})$ states confined by the X_{xy} well. These states are strongly localized in the GaAs layer even at small values of n, confirming the similar findings in GaAs/GaP

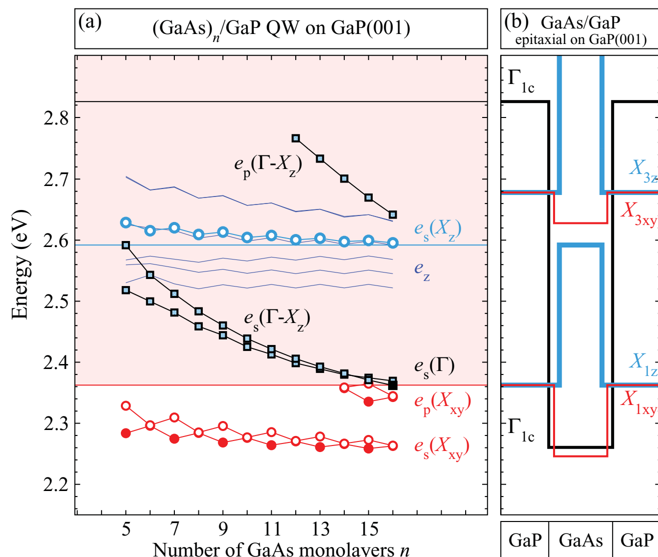

FIG. 10. (Color online) Same as Fig. 8 but for GaAs/GaP epitaxially on GaP(001) and $(GaAs)_n/GaP$ QWs.

SLs,[11] where the biaxially strained GaAs becomes indirect. Note the similarities of $e_s(X_{xy})$ and $e_p(X_{xy})$ in the GaAs/GaP and InP/GaP QWs: In both systems, two sets of states of same spherical symmetry (s or p), appearing in pairs, with an oscillating, n-dependent splitting between them. Because the point symmetry for odd/even n in a common cation system is just the opposite of the common anion (Sec. II D), here the two $\bar{M}$ states are degenerate for n even and split for n odd.

X_z-localized states [open blue (light gray) symbols in Fig. 10]. Similar to the $(GaAs)_n/AlAs$ QW, we find a segregating $e_s(X_z)$ state strongly localized within the GaAs QW and resonant with the GaP continuum. Its energetic position is again slightly above the GaAs (this time strained) X_{1z} edge.

Natural IFLSs. Neither in GaAs/GaP can we observe the appearance of deep IFLSs in the barrier gap. Antiwell X_z states e_z as described above for $(GaAs)_n/AlAs$ are, however, present. The $\Gamma - X_z$ offset for strained GaAs/GaP is only $\simeq 0.1$ eV, a much smaller value than in InP/GaP or even GaAs/AlAs, which explains the presence of the e_z states at relatively high energies above the matrix CBM. Our comparison of InP/GaP QW with varying substrates—GaP(001) versus GaAs(001)—has shown that there is a correlation between the Γ(well)-X_z(matrix) offset and the depth of the IF states. The small value of this offset in GaAs/GaP indicates that the reason for the lack of IFLSs resides in the Γ-electron attraction toward the well being too small.

VIII. CONCLUSIONS

Atomistic empirical pseudopotential calculations revealed the formation of a localized interface state at the InP/GaP heterojunction when this is pseudomorphic to either GaP(001) or GaAs(001). A spectral analysis of this interface state allowed us to interpret it as appearing because of the simultaneous presence of an attracting Γ dip and a repulsive X barrier at the interface. When forming an InP/GaP QW, this interface state evolves into a symmetric-antisymmetric pair of IFLSs, energetically located into the band gap of the GaP matrix. Because of their mixed $\Gamma - X$ character, these states possess a strong optical signature. By calculating the interband absorption spectra, we could show that the IFLSs provide results consistent with the available experimental data, both quantitatively (the position of the absorption peaks) and qualitatively (describing a spatial indirect transition). In the thick QW regime the symmetric IFLS can additionally couple to a conventional Γ-confined, QW-localized electron state giving rise to an even more complicated energy spectrum.

We have further investigated the presence of IFLSs in GaAs/AlAs and GaAs/GaP, other III-V QW systems falling in the class of CB Γ-X interlacing combinations. We have found that IFLSs are present also in these two cases, but, instead of localizing in the gap, they remain resonant with the matrix continuum. Because such IFLSs are detrimental for many optoelectronic devices, acting as recombination centers, we suggest that their presence or absence needs to be verified and, if possible, tuned, for each specific application.

ACKNOWLEDGMENTS

This work was supported by the US Department of Energy, Office of Science, Basic Energy Sciences, under Contract No. DE-AC36-08GO28308 to NREL. V.P. also acknowledges the administrative support of REMRSEC at the Colorado School of Mines, Golden, CO.

APPENDIX: AlAs/GaAs AND InP/GaP/GaAs PSEUDOPOTENTIALS

The screened atomic pseudopotentials $v_\alpha(\vec{r},0)$ entering Eq. (4)

$$v_\alpha(\vec{r},0) = \sum_{\vec{q}} e^{i\vec{q}\cdot\vec{r}} v_\alpha(q), \qquad \text{(A1)}$$

with α denoting the atomic species, have been set up as a Gaussians sum[36]:

$$v_\alpha(q) = \Omega_\alpha \sum_{i=1}^{4} a_i^\alpha \exp\left[-\left|b_i^\alpha\right|\left(q - \left|c_i^\alpha\right|\right)^2\right]. \qquad \text{(A2)}$$

The nonlocal spin-orbit coupling potential term in Eq. (3) has been calculated using the formula[37]

$$\widehat{V}_{\text{NL}} = a_{\text{SO}} \sum_{i,j} |\, i\rangle B(i,j)\langle\, j\,|\,, \qquad \text{(A3)}$$

where $|\, i\rangle$ and $|\, j\rangle$ are reference functions, and $B(i,j)$ is a matrix representation of the spin-orbit interaction, $B(i,j) = \langle i|\,\vec{L}\vec{S}|\, j\rangle$, with $\vec{L}$ and $\vec{S}$ the spatial angular momentum and spin operator, respectively.

Calculations for the $(AlAs)_n/GaAs$ QW employed the pseudopotentials given by Luo *et al.*[36] with a kinetic energy scaling factor $\beta = 1.1$ in Eq. (3). For the other two systems, $(InP)_n/GaP$ and $(GaAs)_n/GaP$, we have used a similar Gaussian fit, with a scaling factor $\beta = 1.23$ and a cutoff of 5 Ry in the Fourier series [Eq. (A1)]. The parameters used for the different atoms in their corresponding binaries are given in Table I. In addition, we list, in Table II, the target values used to fit the pseudopotentials and the corresponding fitted values for the InP, GaP, and GaAs binaries.

TABLE I. Parameters for the screened atomic pseudopotentials used for GaAs, InP, and GaP. Ω is given in (a.u.)^3, all other parameters in atomic units; see (A2) and (A3). A plane-wave cutoff of 5 Ry was used in fitting these potentials. Also listed is the strain fitting parameter γ entering Eq. (4). Numbers in brackets are a form of scientific notation; for example, 5.1346[−09] means 5.1346×10^{-9}.

	Ω	a_{SO}	γ	a	b	c
			GaAs, Lattice constant: 5.6533 Å			
Ga	131.8	5.1346[−09]	0.4558	−2.049 991 09[+00]	1.715 650 28[+00]	0.000 000 00[+00]
				7.164 758 74[−02]	2.946 307 27[−02]	7.354 110 60[−09]
				3.856 523 14[−06]	2.901 070 82[−05]	2.824 113 28[−05]
				−4.430 377 80[−06]	4.525 175 88[+04]	1.062 455 06[+00]
As	75.0	1.4621[−01]	0.0000	−7.258 096 34[−01]	1.278 931 35[+00]	0.000 000 00[+00]
				1.711 100 80[−08]	2.480 896 24[+01]	9.727 849 96[−05]
				2.339 343 68[−01]	1.891 093 76[+00]	1.518 192 74[+00]
				−1.041 398 17[+00]	1.379 048 51[+00]	4.882 919 62[−01]
			InP, Lattice constant: 5.8687 Å			
In	131.8	2.1419[−11]	0.5250	−1.637 360 60[+00]	1.469 886 47[+00]	0.000 000 00[+00]
				2.080 145 97[−01]	1.773 726 03[+01]	1.684 469 70[+00]
				5.300 079 02[−13]	2.149 006 38[−10]	2.017 211 27[−03]
				−4.995 750 59[−03]	2.719 067 66[+01]	7.696 190 77[+00]
P	75.0	5.2427[−02]	0.0000	−1.791 255 00[+00]	1.758 276 71[+00]	0.000 000 00[+00]
				1.821 864 02[−01]	4.451 436 48[−02]	4.042 981 17[+00]
				1.913 284 26[−04]	2.131 874 60[−02]	5.705 169 30[+01]
				−6.974 358 17[−01]	1.011 061 67[+00]	5.194 228 90[−01]
			GaP, Lattice constant: 5.4505 Å			
Ga	131.8	3.4296[−01]	0.4591	−2.159 965 50[+00]	1.970 386 93[+00]	0.000 000 00[+00]
				2.292 184 96[−02]	3.792 460 25[−09]	1.295 027 57[−06]
				5.986 593 08[−07]	2.525 845 21[+01]	3.294 682 23[−05]
				−9.719 646 29[−04]	6.447 117 35[+02]	6.937 537 14[+00]
P	75.0	8.0134[−04]	0.0000	−5.247 245 85[−01]	1.519 181 82[+00]	0.000 000 00[+00]
				4.938 003 25[−09]	2.108 958 75[+01]	1.943 842 52[−03]
				2.978 277 04[−01]	1.227 535 04[+00]	1.618 518 80[+00]
				−9.220 740 74[−01]	1.298 377 05[+00]	7.197 756 80[−01]

TABLE II. Fitted bulk electronic properties for GaAs, InP, and GaP using the screened atomic pseudopotentials (PP) of this work. All energies are given relative to the unstrained $E_{\Gamma_{15v}}$. m_e^*, m_{hh}^*, m_{lh}^* are the effective masses for the electron, the heavy-hole, and the light-hole; $a_{\Gamma_{1c}}$, $a_{\Gamma_{15v}}$ are the hydrostatic deformation potentials at the Γ_{1c} and Γ_{15v} levels; b is the biaxial deformation potential; Δ_0 is the spin-orbit splitting at Γ_{15v}.

	GaAs		InP		GaP	
Property	PP	Target	PP	Target	PP	Target
$E_{\Gamma_{15v}}$ (eV)	−5.628	−5.629 [a,b]	−5.993	−5.989 [a]	−6.098	−6.099 [a]
$E_{\Gamma_{1c}}$ (eV)	1.519	1.519 [b]	1.433	1.424 [b]	2.826	2.895 [c]
$E_{X_{1c}}$ (eV)	1.985	1.980 [c]	2.398	2.380 [d]	2.361	2.350 [c]
$E_{X_{3c}}$ (eV)	2.436	2.500 [c]			2.678	2.705 [c]
$E_{X_{5v}}$ (eV)	−2.964	−2.960 [c]	−2.570	−2.200 [d]	−2.870	−2.700 [c]
$E_{L_{1c}}$ (eV)	1.863	1.810 [c]	1.945	2.030 [d]	2.723	2.637 [c]
$E_{L_{3v}}$ (eV)	−1.221	−1.300 [c]	−1.098	−1.230 [d]	−1.087	−1.200 [c]
$m_e^*(\Gamma)$	0.055	0.067 [b]	0.052	0.077 [b]	0.09	0.13 [b]
$m_e^*(X_{1c,l})$					10.39	10.9 [b]
$m_e^*(X_{1c,t})$					0.19	0.25 [b]
$m_{hh}^*[100]$	0.299	0.35 [b]	0.337	0.52 [b]	0.40	0.54 [b]
$m_{hh}^*[111]$	0.728	0.893 [b]	0.777	0.95 [b]	1.64	0.67 [b]
$m_{lh}^*[100]$	0.082	0.090 [b]	0.071	0.104 [b]	0.14	0.16 [b]
$m_{lh}^*[111]$					0.11	0.17 [b]
$a_{\Gamma_{1c}}$	−6.13	−8.15 [e]	−9.84	−6.40 [e]	−9.16	−8.83 [e]
$a_{\Gamma_{15v}}$	−1.22	−1.21 [e]	−0.58	−0.41 [e]	−0.58	−0.58 [e]
b	−3.61	−2.00 [b]	−2.16	−2.00 [b]	−3.63	−1.60 [b]
Δ_0 (eV)	0.345	0.341 [c]	0.115	0.108 [b]	0.08	0.08 [b,c]

[a]Reference 38; [b]Reference 39; [c]Reference 40; [d]Reference 41; [e]Reference 42.

*voicu.popescu@gmail.com
†alex.zunger@gmail.com

[1]W. Mönch, *Semiconductor Surfaces and Interfaces*, 3rd ed., Springer Series in Surface Sciences, Vol. 26 (Springer Verlag, Berlin, 2001).
[2]W. E. Pickett, S. G. Louie, and M. L. Cohen, Phys. Rev. B **17**, 815 (1978).
[3]J. Ihm and M. L. Cohen, Phys. Rev. B **20**, 729 (1979).
[4]T. Kinoshita, H. Ohta, Y. Enta, Y. Yaegashi, S. Suzuki, and S. Kono, J. Phys. Soc. Jpn. **56**, 4015 (1987).
[5]Y. Hefetz, D. Lee, A. V. Nurmikko, S. Sivananthan, X. Chu, and J.-P. Faurie, Phys. Rev. B **34**, 4423 (1986).
[6]C. R. Leavens and R. Taylor (editors), *Interfaces, Quantum Wells, and Superlattices*, NATO ASI Series B, Vol. 179 (Plenum Press, New York, 1988).
[7]Y. R. Lin-Liu and L. J. Sham, Phys. Rev. B **32**, 5561 (1985).
[8]R. A. Suris, Sov. Phys. Semicond. **20**, 1258 (1986).
[9]S.-H. Wei and A. Zunger, J. Appl. Phys. **63**, 5794 (1988).
[10]F. Hatami, G. Mussler, M. Schmidbauer, W. T. Masselink, L. Schrottke, H.-Y. Hao, and H. T. Grahn, Appl. Phys. Lett. **79**, 2886 (2001).
[11]R. G. Dandrea and A. Zunger, Phys. Rev. B **43**, 8962 (1991).
[12]L.-W. Wang, L. Bellaiche, S.-H. Wei, and A. Zunger, Phys. Rev. Lett. **80**, 4725 (1998).
[13]Y.-T. Lu and L. J. Sham, Phys. Rev. B **40**, 5567 (1989).
[14]D. J. Chadi and M. L. Cohen, Phys. Status Solidi B **68**, 405 (1975).
[15]R. M. Wentzcovitch, M. Cardona, M. L. Cohen, and N. E. Christensen, Solid State Commun. **67**, 927 (1988).
[16]T. N. Morgan, Phys. Rev. Lett. **21**, 819 (1968).
[17]P. Bogusławski and A. Baldereschi, Solid State Commun. **70**, 1085 (1989).
[18]A. J. Williamson, L. W. Wang, and A. Zunger, Phys. Rev. B **62**, 12963 (2000).
[19]A. Zunger, *Quantum Theory of Real Materials* (Kluwer, Boston, 1996).
[20]L.-W. Wang and A. Zunger, J. Chem. Phys. **100**, 2394 (1994).
[21]P. N. Keating, Phys. Rev. **145**, 637 (1966).
[22]R. M. Martin, Phys. Rev. B **1**, 4005 (1970).
[23]K. Kim, P. R. C. Kent, A. Zunger, and C. B. Geller, Phys. Rev. B **66**, 045208 (2002).
[24]V. Popescu, G. Bester, M. C. Hanna, A. G. Norman, and A. Zunger, Phys. Rev. B **78**, 205321 (2008).
[25]V. Popescu and A. Zunger, Phys. Rev. Lett. **104**, 236403 (2010).
[26]I. Tamm, Phys. Z. Sowjetunion **1**, 733 (1932).
[27]W. Shockley, Phys. Rev. **56**, 317 (1939).
[28]H. M. James, Phys. Rev. **76**, 1611 (1949).
[29]W. Trzeciakowski, Phys. Rev. B **38**, 4322 (1988).
[30]F. Hatami, W. T. Masselink, and L. Schrottke, Appl. Phys. Lett. **78**, 2163 (2001).
[31]F. Hatami, W. T. Masselink, L. Schrottke, J. W. Tomm, V. Talalaev, C. Kristukat, and A. R. Goñi, Phys. Rev. B **67**, 085306 (2003).
[32]F. Hatami, V. Lordi, J. S. Harris, H. Kostial, and W. T. Masselink, J. Appl. Phys. **97**, 096106 (2005).
[33]C. V. Dewitz, F. Hatami, M. Millot, J. M. Broto, J. Léotin, and W. T. Masselink, Appl. Phys. Lett. **95**, 151105 (2009).
[34]A. R. Goñi, C. Kristukat, F. Hatami, S. Dreßler, W. T. Masselink, and C. Thomsen, Phys. Rev. B **67**, 075306 (2003).
[35]A. J. Williamson, A. Zunger, and A. Canning, Phys. Rev. B **57**, R4253 (1998).
[36]J.-W. Luo, G. Bester, and A. Zunger, Phys. Rev. B **79**, 125329 (2009).
[37]L.-W. Wang, J. Kim, and A. Zunger, Phys. Rev. B **59**, 5678 (1999).
[38]S.-H. Wei and A. Zunger, Appl. Phys. Lett. **72**, 2011 (1998).
[39]I. Vurgaftman, J. R. Meyer, and L. R. Ram-Mohan, J. Appl. Phys. **89**, 5815 (2001).
[40]O. Madelung, M. Schultz, and H. Weiss (editors), *Numerical Data and Functional Relationships in Science and Technology*, Landolt-Börnstein, New Series, Group III, Vol. 22 (Springer, Berlin, 1997).
[41]T. Mattila, L.-W. Wang, and A. Zunger, Phys. Rev. B **59**, 15270 (1999).
[42]S.-H. Wei and A. Zunger, Phys. Rev. B **60**, 5404 (1999).